Environmental Earth Sciences (2021) 80:407
https://doi.org/10.1007/s12665-021-09487-9

ORIGINAL ARTICLE

Hydrochemistry and environmental isotopes (^{18}O, ^{2}H, ^{3}H, $^{3}He/^{4}He$) of groundwater and floodwater in the great area of Hurghada, Eastern Desert of Egypt

M. Wannous[1] · C. Jahnke[2] · U. Troeger[1] · M. Falk[3] · F. Bauer[4]

Received: 13 July 2020 / Accepted: 4 February 2021

Abstract
Porous and fractured aquifers exist in the area of Hurghada, Eastern Desert of Egypt, whose recharge processes through the common flash floods are not identified. Hydrochemical parameters, stable isotopes ^{18}O, ^{2}H and tritium in floodwater and groundwater were applied in the area subject to study. Additionally, He isotopes were investigated in the deep wells in the faulted zone at the Abu Shaar Plateau. ^{3}H activity in all sampled points lies below the detection limit excluding a recent recharge component in groundwater. However, the hydrochemical ratios and the stable isotope signature confirm that the shallow wells and springs (Red Sea Hills group) are being recharged from modern precipitation. The hydrochemical parameters of the deep wells at the Abu Shaar Plateau (coastal plain group) confirm another origin for the ions rather than the modern precipitation. Together with the ^{18}O and ^{2}H values, the Br/Cl ratio of this group confirms the absence of seawater intrusion component and the role of the fault as a hydraulic barrier. These ^{18}O and ^{2}H values deviate from the GMWL confirming an evaporation effect and colder infiltration conditions and reveal strongly a possible mixing with the Nubian Sandstone in the region. The $^{3}He/^{4}He$ ratio confirms a mantle contribution of 2% from the total He components.

Keywords Groundwater · Floodwater · Hydrochemistry · Water isotopes · Helium isotopes · Eastern desert of Egypt

Introduction

Groundwater is the only available freshwater resource in areas far from the River Nile valley. Its contribution in the water demand of Egypt was estimated at 7% in the time between 1999 and 2002 (Margat et al. 2006). Brackish groundwater in the Eastern Desert is widely used for drinking and irrigation in the remote areas and for the desalinization in the touristic facilities along the Red Sea coast. New agriculture lands irrigated with deep groundwater can be observed recently in some areas along the Red Sea coast. Groundwater occurrence, its chemical and stable isotopes properties in this area have been investigated by several studies (Hefny et al. 1992; Nada et al. 1996; El-Sadek et al. 1998). Some of these studies mentioned that groundwater in the area of the Eastern Desert is of paleometeoric origion and the Nubian sandstone aquifer discharges groundwater into alluvial sediments through faults complex (Sultan et al. 2007) and the upper aquifers of Quaternary and Miocene Sandstone are partially recharged from the flash flood (Awad et al. 1996; El-Sadek et al. 1998; Sultan et al. 2007). Several studies have applied the noble gas technique in groundwater investigations in the Eastern and Western Desert of Egypt. Sturchio et al. (1996) investigated the thermal groundwater discharged from springs along the Gulf of Suez where Helium was analyzed in Hammam Faroun with an estimation of 3.5% of magmatic He. Sturchio et al. (2004) investigated groundwater age of the Nubian sandstone aquifer at five oases in the Western Desert of Egypt using Kr^{81}.

✉ M. Wannous
m.wannous@mailbox.org

1 Central Institute of Campus El Gouna, Department of Water Engineering, Technische Universität Berlin, Ackerstraße 76, 13355 Berlin, Germany

2 Mecklenburg-Western Pomerania State Office for the Environment Nature Conservation and Geology, Goldberger Str. 12, 18273 Güstrow, Germany

3 Museum of Natural History, Leibniz Institute for Evolution and Biodiversity Science, Invalidenstraße 43, 10115 Berlin, Germany

4 Karlsruher Institute of Technology, Campus Nord, Hermann-von-Helmholtz-Platz 1Eggenstein-Leopoldshafen, 76344 Karlsruhe, Germany

Published online: 28 May 2021

Aeschbach-Hertig et al. (2006) investigated the recharge and the paleometric temperature of groundwater in the area of Nile Delta using s spectrum of noble gases.

The investigation area is located between Hurghada city in the south and Wadi Melaha Oasis in the north at the Red Sea coast of Egypt (Fig. 1). Abu Shaar Plateau exists around 22 km south of Wadi Melaha Oasis and 5 km west of El Gouna (Fig. 1). At the fault zone which separates this plateau from the coastal plain (Klitzsch and Linke 1983) several wells were drilled between 1994 and 2000 (Kleinendorst 2004) to pump brackish water to supply El Gouna area. Moving southwards to the area extended between El Gouna to 36 km SW of Hurghada city, several springs and shallow wells (Fig. 1) provide small communities in the Eastern Desert with water. The springs and some wells exist in the basement rock formed by Precambrian fractured granite while other wells are in the Quaternary alluvial deposits which settled between the basement hills. Deep wells used mainly to irrigate new agriculture farms can be observed in the area of Wadi Om Dehas (Fig. 3). In Wadi Melaha Oasis north of El Gouna (Fig. 1) a permanent spring and a stream could be detected.

The purpose of this study is to investigate the processes which influence the hydrochemistry of groundwater and their stable isotopes values in the area and weather the flash floods which are common in the region contribute to the groundwater recharge.

Natural conditions of the study area

Geological and tectonic settings of the study area

The study area is located at the southwestern border of the Gulf of Suez. The rifting in the Gulf of Suez evolved in the Late Oligocene and Miocene and is to a minor extent still active (Bosworth et al. 2005). Faults and fractures zones (ENE-WSW) strike the different blocks in the area which resulted from the subsidence of the Red Sea Graben (Bosworth and Taviani 1996). The stratigraphy in the investigated area can be divided into three major sedimentary units (Klitzsch and Linke 1983):

- Pre-rift units (Pre-Oligocene) which include Gr basement (Precambrian Granites), Palaeozoic, Upper Cretaceous and Lower Eocene;
- Syn-rift Units (Late Oligocene–Middle Miocene) which include Tmm Middle Miocene (continental and shallow marine), Tev Evaporates of Middle and Late Miocene;
- Late-rift units (Late Miocene/Pliocene to Quaternary) represented in Tpl Pliocene (shallow marine and continental clastic rocks) and Q, QG, S, W Quaternary (gravel plain, sabkha deposits, alluvial fan and wadi deposits.

The basement in the north of the Eastern Desert, where the study area is located, is relics of the Neoproterozoic orogeny (Stern and Hedge 1985). The magmatic rocks are separated into two groups, granitoids and volcanic (Greilling et al. 1988). The rocks are exposed to the surface in the mountainous areas of the Red Sea Hills, forming very steep and high mountain ridges. The Red Sea Hills in the area are formed by Precambrian crystalline basement (acidic plutons and ophiolite formations) (Greilling et al. 1988; Hadidi 2016). Paleozoic and Mesozoic discordant layers are mostly continental and shallow marine sandstones (Alsharhan 2003), including the Nubian sandstone, which is known as the most productive aquifer in the western desert (Thorweihe and Heinl 2002) but disconnected from those sources in the Eastern desert.

The sedimentary environment changed in the beginning of Cretaceous times and gradually moved from continental to the marine environments of the Eocene, which is dominated by thick limestone formations.

Tertiary is the time of the main phase of uplifting (Miocene) and mostly sedimentary rocks are originated in the syn-rift period.

The syn-rift sediments in the investigation area range from siliciclastic in the Early and Middle Miocene (coarse conglomeratic fan deltas, close to active fault systems and uplifted blocks, to the distal fine-grained clastic material) to shallow marine limestones and evaporates in the Late Miocene (Bosworth and McClay 2001).

After Hadidi (2016) and Linke (1986) halite which is intersected with sulphate and carbonates (evaporates units Tev, Fig. 1) form thick evaporitic sequence is responsible for the high salinities in the deep brines of the Red Sea. The halite has been washed out near the surface and the evaporates consist mainly of gypsum and anhydrite.

Post-rift strata overlying most of the syn- and pre-rift deposits. The Pliocene and Quaternary soft rocks mainly consist of fanglomeratic gravels and sands (Bosworth 1996) with locally very huge thicknesses. The coarse-grained layers, deposits of evaporates, limestones and marls are widely spread and separate different lithologically and hydrogeological units.

The Abu Shaar Plateau consists mostly of carbonatic formations of the Middle Miocene (Fig. 1) and is located along the main fault system in direction NW–SE. Very steep slopes differentiate the plain from the mountainous areas which highest elevations reaches more than 200 m a.s.l. (Gebel Abu Shaar). To the north crystalline basement outcrops at the surface. The area of the coastal plain is shallow (5 and 20 m.a.s.l). It consists of the Late-Rift sequences of the Pliocene and Quaternary, which are composed of alluvial fan and wadi deposits (QW), gravel plain deposits (QG), sabkha deposits (Qs) and shallow marine clastics (Tpl and Q) with

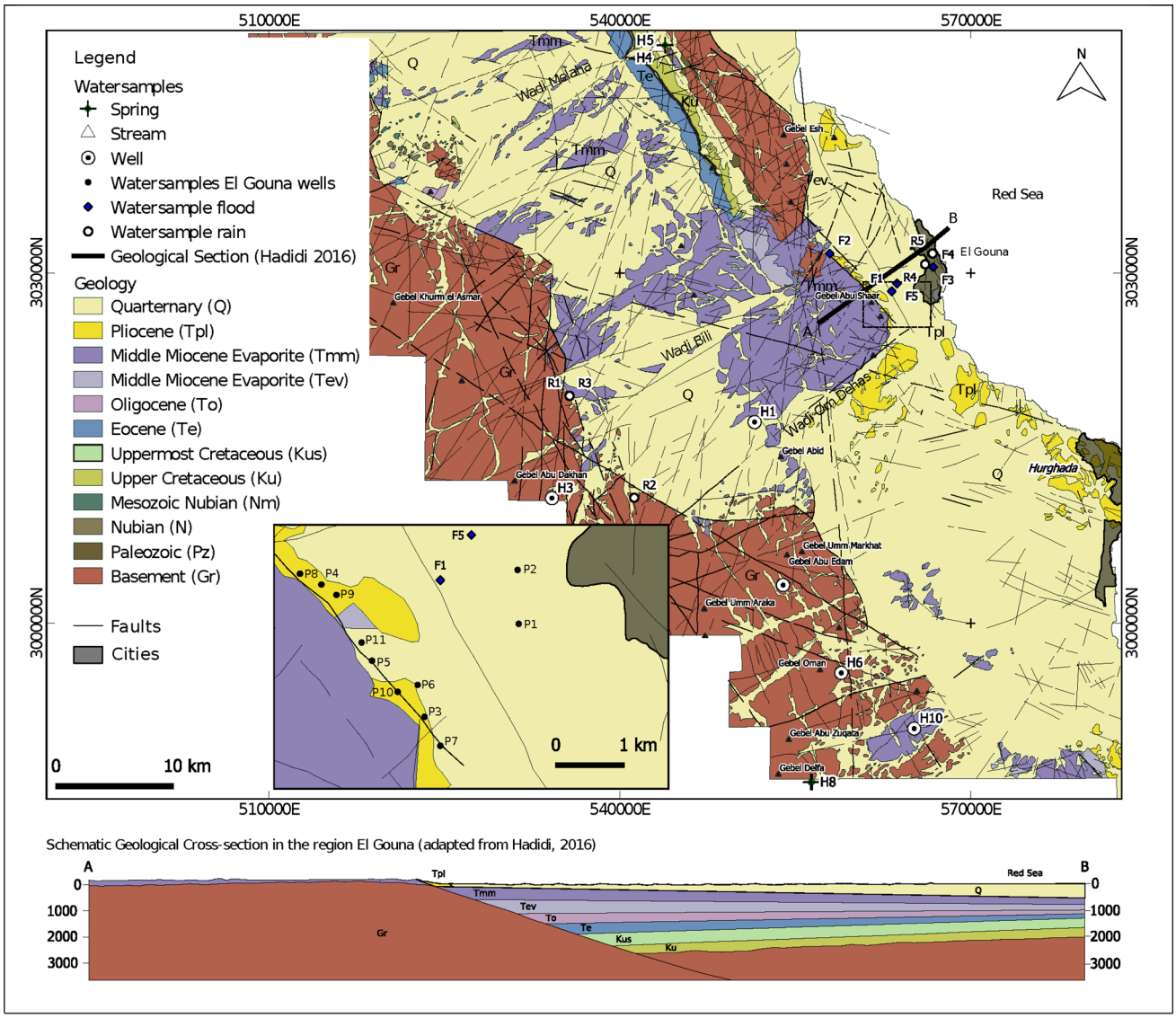

Fig. 1 Geological map of the area modified after Klitzsch and Linke (1983) (coordinate system: ETRS, 1989 UTM 36N, epsg-code: 25836, also in the following maps)

thicknesses up to several 100 m (Hadidi 2016; Klitzsch and Linke 1983).

Hydrogeology

The classification of aquifers is according to the tectonic phases distributes the aquifers system into basement, pre-rift, syn-rift and post-rift aquifers. All aquifers are present in the study area.

The mountainous area of the Red Sea Hills is dominated by magmatic basement aquifer represents the pre-rift aquifer. These rocks form fractured aquifers which can be of greater thicknesses and good transmissivities in fault zones (Salah and Alsharhan 1996). The basement aquifer can be connected to springs and old wells along the basement faults delineate water resources (Hadidi 2016). The availability of aquifers of the pre-rift phase is limited.

The Syn-rift aquifers of pre-Miocene and Miocene are present at the Abu Shaar Plateau west of El Gouna. The carbonatic formations are conductive and can be karistified (Hadidi 2016).

The post-rift aquifers of Pliocene and Quaternary are present in the coastal plains and east to Abu Shaar in the area of El Gouna and Om Dahes valley (Fig. 1). The shallow porous aquifers are separated by thin silty layers. The aquifers consist of sandy, locally fine grained and silty parts, often interlaced by gravel and coarse sands (Hadidi 2016). The extensive geophysical exploration carried out by Sultan

et al. (2011) shows structures and relation to groundwater in the coastal plain of the Egyptian Red Sea coast and in parts of the Red Sea Hills. An important focus was the measurements along the NE and SW ridge of wadi Melaha (Fig. 1). Three deep depressions in this area were delineated that seem to be important for the storage of groundwater. Tectonic structures link these depressions. The deepest depression west of Abu Shaar Mountain has an estimated depth of 2340 m. The topographic altitude of the area is between 120 and 200 m.a.s.l while the coastal plain has a topographic altitude between 0 and 70 m. The hydraulic role of the faults will be discussed in Sect. 5.

Climatology

The climate in the Eastern Desert of Egypt is arid and generally characterized by hot summers and moderate winters. Most of climate stations which are installed in the Eastern Desert are located at the coastal line and they reflect the coastal effect which moderates the temperature (Hadidi 2016). The climate data presented in Fig. 2 were obtained from a climate station located at the Red Sea coastal plain (27.43 E, 33.66 N) which is located on an elevation of 4 m.a.s.l. The calculated monthly averages are based on a measuring period between March 2014 and January 2019 with a time interval of 10 min.

The seasonal trend shows the highest temperatures between June and August (> 30 °C) and the lowest in December and January (< 20 °C). The relative humidity with an annual average of 47% also shows a weak seasonal variation with a minimum between May and August (average 45%) and a maximum between October and December (average of 50%).

Sporadic precipitation events take place in winter months (between October and April) having durations of a few minutes to few hours. During 2014 and 2018, three events with a precipitation > 10 mm occurred and could be recorded in El Gouna weather station (08/09-03-14: 33 mm, 25–10-15: 10 mm, 27-10-16: 20 mm). These events led to flash floods in the Red Sea Hills and the coastal plain (Hadidi 2016; Saber et al. 2020). Five other events with precipitation < 1 mm without floods were recorded additionally. The precipitation and flood events could partially be sampled for chemical analyses (Sect. 4.1, Table 1).

Evaporation data from the region were reported by Awad et al. (1996) with a maximum annual mean value in June with 10.11 mm/day and a minimum in December with 6.11 mm/day.

Methodology

Sampling and chemical analytics

Water sampling: chemical and isotopes analytics

Samples from rainfall, floodwater, groundwater, and seawater were analyzed in the time between 2014 and 2019 to investigate the origin and quality of groundwater in the investigation area. The intense precipitation event of March 2014 and the resulting flash flood could be sampled at several locations (rainwater samples R1–R3, floodwater samples F1–F3, Fig. 3, Table 1). The field parameters have not been measured during this sampling (Askar 2014; Hadidi 2016). The rain gauges where samples R1, R2, R3 have been manually installed in the mountain ridge (Fig. 3). Rain depth at R1 was measured on 03-03-2014 with 7 mm, while the rain depth on 09-03-2014 in R2 and R3 locations was measured with 32 and 47 mm, respectively (Hadidi 2016). Additional rainwater and floodwater samples were collected in

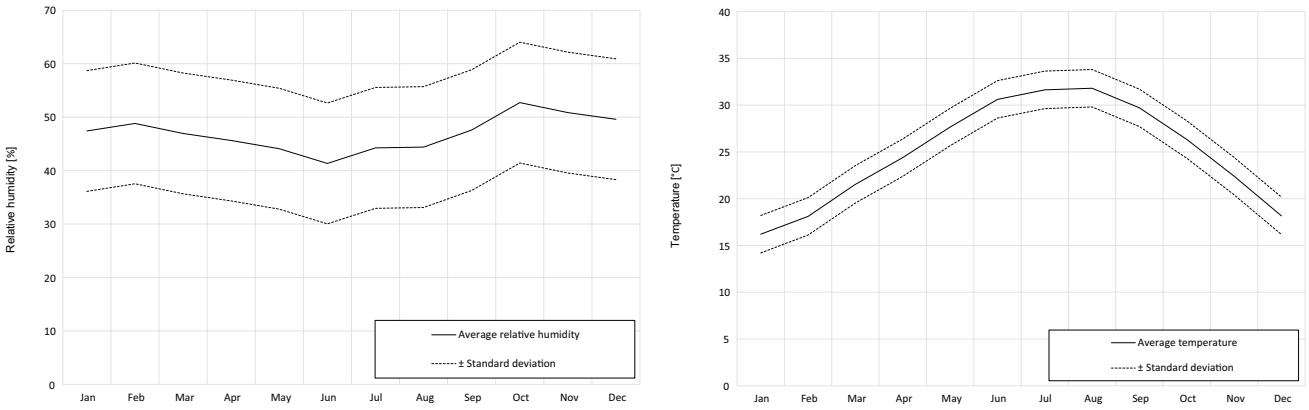

Fig. 2 Temperature (left) and relative humidity (right) record in El Gouna climate station (based on 10 min-timerow data Oct/2015–Feb/2019)

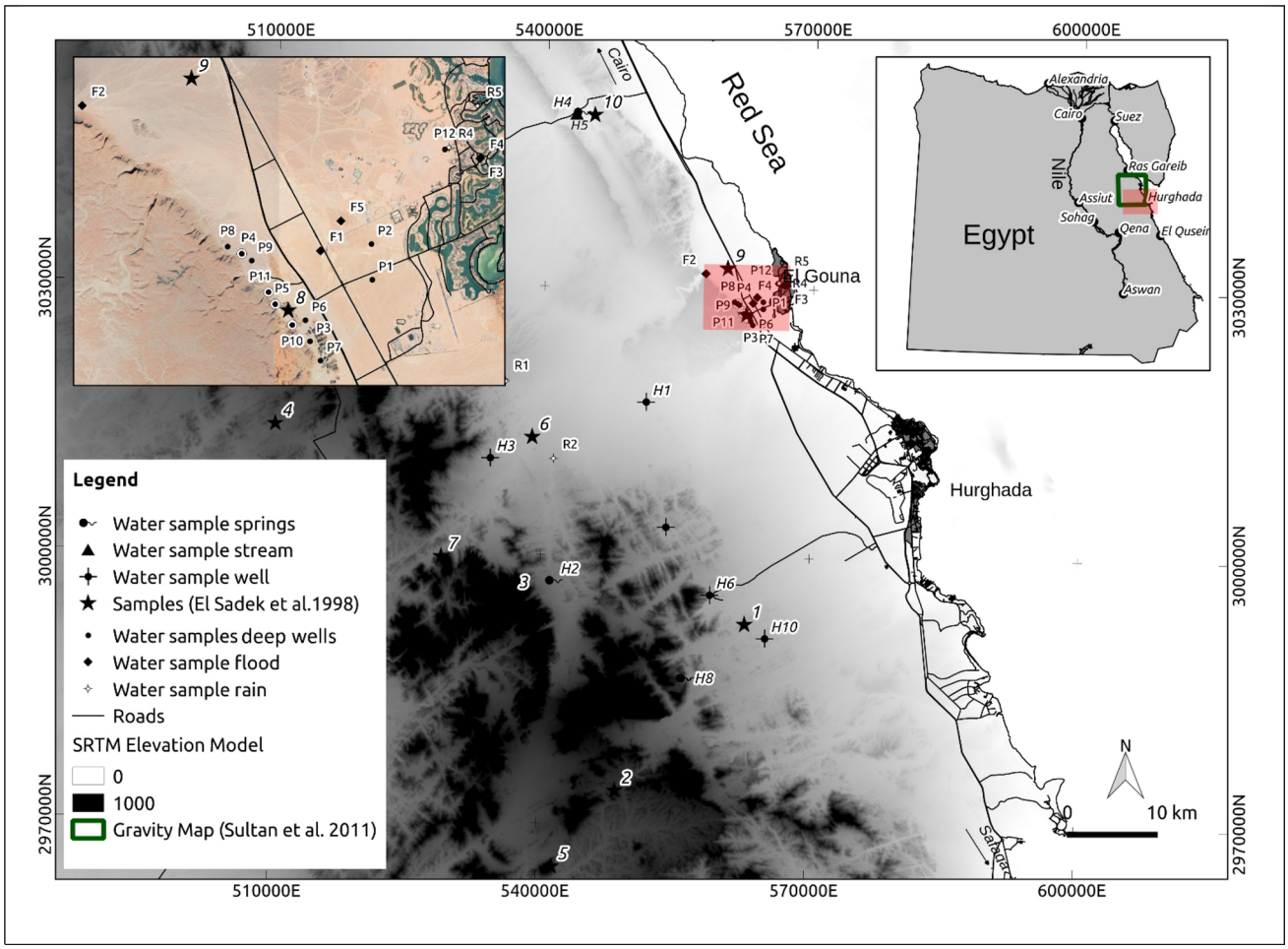

Fig. 3 Investigation area: locations of the coastal plain group and the Red Sea Hills group

October 2016 (R4, F4–F6) from the rainfall event of 20 mm. In February 2018 sample (R5) was collected from the rainfall event of 3 mm and in February 2019 sample (F7) from a rainfall event in Wadi Araba area (Fig. 3, Table 1). Beside the field parameters which were measured in all samples, the alkalinity was also determined in the field.

Groundwater samples have been collected from the existing springs and wells in the study area. The samples were divided into two regional groups:

The coastal plain group (samples P1–P9) which includes 20 wells, nine of them were sampled for this study (Tables 1 and 2). They are located 5 km west of El Gouna and they will be referred as "deep wells" in the rest of this study. These wells were drilled in the time between 1990 and 2000 and belong to the aquifer of Pre-Miocene and Miocene with carbonatic-silicastic sequences which belong to the syn-Rift units. Information records about the well constructions data aren't available. The locations of the wells were determined using a GPS device with accuracy of ± 5 m. Measuring the water table in the field was not possible due to the permanent pumping. Well heads are not referenced to a vertical datum. The wells have depths between 30 and 140 m (Table 1) and are used for water supply and irrigation purposes.

The Red Sea Hills group (samples H1–H10) which belongs to wells (four shallow dug wells with depth from 10 to 33 m and one drilled deep well), four springs and a permanent stream of Wadi Malaha Oasis (Table 1). The springs H2, H8, H9 belong to the crystalline basement of the Red Sea Hills. H4, H5 belong to Melaha spring and stream of an oasis at the north of El Gouna, Fig. 1. All these springs have low flow rate which could not be quantified in the field. Samples H3, H6, H7 in this group belong to dug wells exist in the wadi sediments of the late-Rift units. H1 is a drilled well of 300 m depth and irrigate a citrus farm. Four additional wells adjacent to H1 were detected during the sampling campagna but could not be sampled. H10 belong to a well of 15 m depth drilled in the basement on a fracture.

The parameters EC, T, pH were measured at each sampling location using WTW portable devices. Total and carbonate hardness was measured in the field using gran titration. For all samples of rainwater, floodwater sampled in and after 2016 and groundwater, anion and cations samples were filtered in the field using 0.45 µm filter and filled into 50 ml bottles. The cation and anion samples were acidified by adding 0.2 ml of HNO_3 and 0.2 ml of bacteria acid C4H8N2S, respectively. NO_3, SO_4, Cl and Br were analyzed using a Metrohm® 881 Compact Ion Chromatograph pro-Anion –MCS. Major cations (Ca, Mg, Na, and K) were analyzed using an Agilent® 715 ICP-OES. All analyses were performed at a laboratory on the El Gouna campus of the Technical University of Berlin, Egypt.

Nine samples from the coastal plain group, eight samples from the Red Sea Hills group, one rainfall sample were collected for determining the stable isotopes ($^{18}O/^{16}O$) and hydrogen ($^{2}H/^{1}H$) in H_2O by filling water into 2 ml bottles, finally sealed to prevent evaporation according to IAEA (2009). Stable isotope ratios of oxygen ($^{18}O/^{16}O$) and hydrogen ($^{2}H/^{1}H$) in H_2O in water samples were measured with a PICARRO® L1102-i isotope analyzer at the Museum of Natural History in Berlin, Germany.

The L1102-i is based on the WS-CRDS (wavelength-scanned cavity ring down spectroscopy) technique (Gupta et al. 2009). Measurements were calibrated by the application of linear regression of the analyses of IAEA calibration material VSMOW, VSLAP and GISP. The stable isotope ratios of oxygen and hydrogen are expressed in the conventional delta notation ($\delta^{18}O$, δD) in permil (‰) versus VSMOW. For each sample, six replicate injections were performed and arithmetic average and standard deviations (1sigma) calculated. The reproducibility of replicate measurements is generally better than 0.1 ‰ for oxygen and 0.5 ‰ for hydrogen.

Seven samples from the coastal plain group were collected to analyze the tritium ^{3}H and the noble gas Helium He. Groundwater from the Red Sea Hills group could not be sampled for He. All dug wells and springs in this group are open and have contact with the air. Therefore, only samples for ^{3}H were taken from this group. For this purpose, each sample was filled into one 1000 ml bottle. The measurements were carried out by applying the electrolytic enrichment using Liquid Scintillation Counting (LSC) in Hydroisotop Laboratory, Schweitenkirchen Germany. Values are reported in tritium units (TU) where 1 TU equals an activity of 0.119 Bq/L (IAEA 1992) and tritium half-life time is (4500 ± 8) days (≈12.3 years) (Lukas and Unterwegers 2000). The detection limit is 0.5 TU.

For ^{3}H and He sampling in the coastal plain group, each sample was filled into two 40 ml gas tight copper tubes.

The sampling was performed by connecting the groundwater coming out of the wells to a transparent flexible tube which is in turn connected with the copper pipe. The other end of the copper pipe was connected as well to another transparent tube. This sampling procedure enables the sampler to prevent mixing the air bubbles with groundwater. The tube was flushed at least ten times before filling it with sampled groundwater. The pipe two ends were screwed properly. In the same time, and for each well which was sampled for He, another bottle of 1000 ml size was filled with groundwater for the ^{3}H analysis. Tritium measurements of the coastal plain group were carried out together with He and Ne at the Institute of Environmental Physics, laboratory of noble gases, University of Bremen, Germany. The measurement method was developed by Sultenfuss et al. (2009) and has precision of ± 3% with a detection limit of 0.015 TU for 500 g water (storage time 3 months).

After gas extraction in the laboratory, Ne and He isotopes were purified in a two level cryo system at 25 and 14 K. ^{4}He, ^{20}Ne, and ^{22}Ne were measured with a Quadrupole mass spectrometer (Pfeiffer QMG 112). After separation from Ne, ^{3}He, and ^{4}He were analyzed with a high-resolution sector field mass spectrometer (MAP 215-50). The typical precision for He and Ne concentration is better than 1%. Ne is measured to determine the atmospheric He component. Salt corrections were made assuming an initial equilibrium in fresh water.

Soil samples and XRD analytics

Two soil samples of clay collected from the alluvial fan of Wadi Bili Fig. 1 were analyzed using D2 Phaser. The wadi mud sample was collected from the protection depression where the flood water is collected after heavy rainfalls. The second sample was taken from a drilling location in the area of El Gouna at a depth of one meter under the surface. The samples have been crushed into a powder (< 63 µm) and finally analyzed in the institute of applied geochemistry at the Technical University of Berlin, Germany.

Evaluation methodology

Hydrochemical development

The hydrochemical processes and the development of the water quality from precipitation to floodwater and groundwater are discussed by means of $\delta^{18}O$, δD and the dissolved ions (Sect. 4.2).

Separation of helium components

The three components of atmosphere, mantle, and crust can be separated according to the simplified model of (Castro 2004; Aeschbach-Hertig 2005; Kaudse 2014):

$$R_s = \frac{^3He_s}{^4He_s} = \frac{^3He_c + ^3He_m + ^3He_a}{^4He_c + ^4He_m + ^4He_a}, \quad (1)$$

where $R_s = {}^3He_s/{}^4He_s$ is the mixture ratio of the He isotopes in the sampled water, c, m and a refers to the ratios R in the crust, mantle, and atmosphere.

Using $^3He/^4He$ ratios for the single components R_A, R_c, R_m, Eq. (1) can be written as:

$$R_s = \frac{^4He_cR_c + ^4He_mR_m + ^4He_AR_A}{^4He_s} = X_cR_c + X_mR_m + X_aR_a. \quad (2)$$

With Xi relative share of ^4He_i in the single fractions $Xc + Xm + Xa = 1$ and the crustal share Xc can be expressed as $Xc = 1\text{-}Xm\text{-}Xa$. Applying this in Eq. 2 results in

$$R_s = \left(1 - X_m - Xa\right)R_c + X_mR_m + X_aR_a, \quad (3)$$

$$X_m = \frac{R_s - R_c - X_a(R_a - R_c)}{R_m - R_c} \quad (4)$$

X_m is mantle fraction of ^4He but not of ^3He. The mantle fraction of ^3He y can be essentially calculated as (Aeschbach-Hetig 2005):

$$Y_i = \frac{^3He_m}{^3He_s} = \frac{^4He_iR_i}{^4He_sR_s} = X_i\frac{R_m}{R_s} \quad (5)$$

The ratio $R_m = {}^3He_m/{}^4He_m$ of the mantle component could be derived from analyses of the Red Sea Deep water from (Winckler et al. 2001) (R_m: 1.3×10^{-5}, $R_m/R_a = 9.2$, with R_a $^3He/^4He$ ratio of the atmosphere 1.38×10^{-6}). The ratio $R_c = {}^3He_c/{}^4He_c$ of the crustal component was assumed to be a crustal average 2×10^{-8} ($R_c/R_a = 0.0145$) (Mamyrin and Tolstikhin 1984). The fractions of Earth mantle and Earth crust of the coastal plain group samples are discussed in Sect. 4.3.

Noble gas equilibrium temperatures

Excess air and the equilibrium temperature can be determined using the Ne concentrations in groundwater (Aeschbach-Hertig et al. 1999). The groundwater content of noble gases includes the gas content derived from the atmosphere and the atmospheric content which is called excess air and this component get less in the heavy gases (Kaudse 2014). In addition to ^3He, ^4He, ^{21}Ne has been analyzed in the samples of the coastal plain group (Table 2). Ne analysis is usually made to estimate the degassing or excess air in the sample. The atmospheric content of noble gas in the rainfall is dependent on the temperature, the salinity and pressure (Kipfer et al. 2002), therefore, the reconstruction of these conditions is possible using the concentrations of noble gases in the aquifer (Bath et al. 1979).

After Aeschbach-Hertig et al. (1999), the initial concentration of the atmospheric noble gases in groundwater is given by

$$C_i^{init} = C_i^{eq}(T, S, P) + A.z_i.\exp\left(-R\frac{D_i}{D_{Ne}}\right), \quad (6)$$

The C_i^{eq} is the equilibrium concentration which is dependent on the temperature T, salinity S and pressure P.

Henry's law describes the partitioning at the air–water interface in term of the concentrations gas in air and water are proportional to each other's.

$$\frac{C_i^{gas}}{C_i^{water}} = H_i(T, S). \quad (7)$$

After Kipfer et al. (2002), this equation is formulated for each gas depending on the partial pressure and the equilibrium concentration:

$$P_i = C_{i,eq}.H_i. \quad (8)$$

The partial pressure P_i of the gas depends on the total pressure of the air P_{tot} which is corrected for the water vapor content $e_w(T)$, and the mole fraction Zi of the gas in the dry air (Kipfer et al. 2002; Ozima and Podosek 1983; Weiss 1970; Weiss and Kyser 1978):

$$P_i = Z_i.\left[\sum\nolimits_i P_i - e_w(T)\right] = Z_i.\left[P_{tot} - e_w(T)\right]. \quad (9)$$

The local barometric altitude effect on the atmospheric pressure is influenced by the local and the sea level pressure:

$$P_{tot}(h) = P_{tot}^{sl}.e^{-h/h_{atm}}, \quad (10)$$

where the P_{tot} together with the saturation vapor pressure should be corrected.

Depending on this model, the atmospheric equilibrium concentrations for He and Ne of the rainfall in dependency of air temperature and topographic altitude can be reconstructed.

Results

Analytical results

Table 1 shows the chemical and stable isotopes ^{18}O, ^2H results for the sampled wells and springs in addition to the rain and floodwater samples.

Table 2 shows the analytical results of ^3H and He isotopes.

The electrical conductivities of all groundwater samples are in the range of brackish water. The values in the deep wells (7.3–19.6 mS/cm) of the coastal plain group differ

from those in the Red Sea Hills group (1.2–4.8 mS/cm) with the exception of H4, H5 and H10. Temperature T differs between the two groups too. While the Red Sea Hills group reflects the air temperature, a thermal influence with elevated temperatures up to 38 °C (Table 1) can be recognized.

Hydrochemistry

Stable isotopes

The northern Red Sea A sample from the northern Red Sea (S1 Table 1) was taken in El Gouna in October 2016 (blue pyramid in Fig. 4) and yielded isotope values of $\delta^{18}O$ 2.3‰ and $\delta^{2}H$ 11.6‰. Isotope values from the Global Seawater Oxygen-18 Database-v1.22 (Schmidt et al. 1999) and scientific literature (Biggs and Rohling 2000; Kürten et al. 2019) confirm the isotope values of sample S1 and reveal an increasing enrichment in $\delta^{18}O$ from the southern to the northern part of the red sea.

Precipitation To construct the LMWL of rainfall, the average content of $\delta^{18}O$ ‰/$\delta^{2}H$ ‰ in rainfall samples from Cairo, Alexandria, Alarish, Marsa Matruh, Rafah, Ras Eltine, Sidi Barrani and St. Catherene (IAEA 2019) was considered. These samples are plotted in Fig. 4. (light blue squares). The LMWL plot as an evaporation line with a slope less than 8 and crosses the GMWL at approximately $\delta^{18}O$ ‰/$\delta^{2}H$ ‰: − 0.3/7 which represents the isotopic values of the mean weighted local precipitation (Gibson et al. 1993). The d-excess of the LMWL (+9.9) indicates evaporation at a relative humidity of approximately 75% (Pfahl and Sodemann 2014).

One rainfall sample in El Gouna could be taken for isotopic analyses in February 2018, R5, weak rainfall event 23-2-18 9:00 pm–24-2-18 1:00 am, ≈3 mm). The cumulative sample was taken overnight in an open vessel and collected next day. The sample is influenced by evaporation (conditions: temperature 17.5–22.3 °C, relative humidity: 60–82%). A floodwater sample could be taken from Wadi Araba area in February 2019. (Table 1, F7, 3 days after a rainfall event). This sampled location is approximately 170 km far to the north. The samples R5 and F7 are plotted in Fig. 4 and reported in Figs. 1 and 3.

To complete the isotopic record of precipitation, additional data from the Red Sea area and its surrounding were taken from literature: Two data were reported by Awad et al. (1996): Qusier–Safaga area $\delta^{18}O$ ‰/$\delta^{2}H$ ‰: − 0.8/ + 1.9, average Khartoum meteorological station (IAEA 2019: $\delta^{18}O$ ‰/$\delta^{2}H$ ‰: − 2.11/− 9.5). Two further samples were reported in by Eissa et al. (2013) and Abdel Samie and El-Sadek (2001) from Sinai Peninsula.

($\delta^{18}O$ ‰/$\delta^{2}H$ ‰: − 4.37/− 21; − 4.3/− 17.1). A rainfall sample from Jedda in Saudi Arabia at the eastern side of the Red Sea was reported by IAEA (2019) $\delta^{18}O$ ‰/$\delta^{2}H$ ‰: 0.88/12.6. In general, these data (yellow rhombs in Fig. 4a) and the floodwater sample F7 (dark blue square in Fig. 4a) plot close to the LMWL. The analyses from the Sinai Peninsula (Abdel Samie and El-Sadek 2001) that represents the source of the local groundwater recharge (Eissa et al. 2013) plot closer to the EMWL the Eastern Meteoric water line (Gat and Carmi 1970) which implies inland conditions and a more arid vapor source. The precipitation sample from El Gouna (R5, Table 1) differs strongly from the LMWL and GMWL and plot on an evaporation line. Regarding an average relative humidity of 70% during the evaporation process (increased humidity during and after the event), the slope of this evaporation line can be approximated with 4.98 (Gonfiantini 1986). Assuming a steady evaporation at 70% humidity, the initial water would plot where the 70% evaporation line crosses the LMWL (Bowen et al. 2018).

Evaporation processes Beside the precipitation sample (R5) also other samples show evaporation effects (Table 1): the stream of the Oasis Wadi Melaha H5, the dug well in Elojaira H10 and the superficial water of Red Sea S1 shown in Fig. 4a.

The source of evaporated stream water sample H5 is sample H4, the spring of Wadi Melaha. The concentration of the conservative parameters Cl and Br are increased by factors of 2.8 and 3.2 from H4 to H5 (Table 1), which means the water loss of the primary solution caused by evaporation is 65–68% (neglecting the sparse precipitation). The slope of the evaporation line between H4 and H5 is 4.74, what can be related to a relative humidity of ≈60% (Gonfiantini 1986). This humidity value is reliable for the air above a watershed in this Oasis. The average isotopic composition of the evaporated water can be calculated to $\delta^{18}O$: − 10.1‰, $\delta^{2}H$: − 69.4‰.

The slope $\delta^{18}O/\delta^{2}H$ of the rainfall samples R5 considering the average Cairo weather station rain ($\delta^{18}O$: − 1.44‰, $\delta^{2}H$: − 4.19‰) as the origin rain. The slope of the evaporation line between R5 and Cairo sample to the GMWL is 4.99 what can be related to a humidity of 70%. This humidity is reliable for an evaporation process above the open Sea. For the dug well Elojaira exist only the evaporated samples H10. In addition, this sample is the only one that shows a Tritium activity above the detection limit (0.7 TU, see Table 2). The well is located in the Red Sea Hills approximately 15 km from the coast (Fig. 3). Using an average relative humidity of 50% (annual average in the coastal area is 47%, Sect. 2.3) results in a slope of 4.45 of the evaporation line in $\delta^{2}H/\delta^{18}O$ relation (Gonfiantini 1986). The primary solution can be extrapolated to more depleted water in a range $\delta^{18}O$: from − 6.5 to − 5‰ and in $\delta^{2}H$: from − 35 to − 45‰ (probably close to isotopic composition of the wells H1 and P8). Comparing with the enrichment in Wadi Malaha (H4, H5) and

Table 1 Hydrochemical and stable isotopic parameters of rainwater, floodwater and groundwater

	Aquifer	X (UTM)	Y (UTM)	Well depth [m]	Sampling date	T [°C]	EC [mS/cm]	pH [-]	Cl [mg/l]	NO_3	SO_4	HCO_3	Br	F	Ca	Mg	Na	K	$\delta^{18}O$ [‰ SMOW]	$\delta^{2}H$
Rain water																				
R1		535705	3019469		03.03.2014				26.2	30	16.6			0.9	41.55	3.3	11.6	3.2		
R2		541232	3010748		09.03.2014				6.3	0.9	2.6		0.4	0.588	7.1	0.1		0.3		
R3		535705	3019469		09.03.2014				8.8	0.5	4.8		0.4	0.674	17.9	1.4		0.6		
R4		566112	3030731		27.10.2016	25.1	0.4	6.5	54	12.3	43.9	17.4	0.1	0	31.5	3.1	21.2	0.9		
R5		566749	3031656		23.02.2018				19.7	0	25.5		0.1	< 0.01	28.4	2.6	14	4.4	3.7	22.0
Flood water																				
F1		563254	3028429		10.03.2014				86.8	36.9	390.1				215.8	31.9	113.1	16.8		
F2		557952	3031661		09.03.2014				76.8	31.9	234.5		0.4	2.51	190.9	20.5	53.7	16.3		
F3		566803	3030486		10.03.2014				214	13.6	499.9				239.4	19	156.2	12.4		
F4		566819	3030495		28.10.2016	25.3	0.6	7.8	61.4	12.7	159	91.5	0	0.196	79.6	7.7	93.3	14.8		
F5		563710	3029094		29.10.2016	25.9	1.2	7.8	175	1.9	278	78.4	0.2	0.346	147	14	130	11.6		
F6		563710	3029094		03.11.2016	22.8	1.2	8.2	184	18	369	91.5	0.1		148	14.9	98.2	13.8		
F7		437557	3200053		18.02.2019		3.5	7.7	659	17.7	799	191.7	0.4	< 0.01	358	33.3	415	18.8	0.7	14
Red Sea Hills																				
H1 (Irrigation farm)	Alluvial sediments	551529	3017229	150	23.02.2019	29.3	2.1	7.5	664	23.5	488	152.5	3.6	< 0.01	145	24.1	262	3.9	− 5.9	− 42
H2 (Om Nfieh)	Basement rocks	541571	2997108	Spring	23.02.2019	15.2	1.2	8.5	157	2.9	161.5	270.1	0.7	5.8	60.3	16.5	180	3.4	− 1.7	− 6.3
H3 (Albadieh)	Alluvial sediments	534193	3010714	10	23.02.2019	23	2.4	8.2	426.6	73.3	443	154.7	0.5	5	112	21.7	391	5.8	− 2.8	− 14.1
H4 Wadi Melaha Spring	Alluvial sediments	543871	3049496	Spring	23.02.2019	23	17.5	7.7	5700	0.4	1910	228.8	61.3	1.5	1314	572	1870	57.6	− 6.2	− 50.5
H5 Wadi Melaha stream	Alluvial sediments	543240	3049305	Stream	23.02.2019	21.9	41.7	8.2	16,000	0.2	2900	126.4	195	3.4	2490	1470	5120	194	1.8	− 12.7
H6 (Om Agira)	Alluvial sediments	553959	3003277	19	22.02.2018	22.6	4.8	8.1	1320	31.9	475	108.9	8.8	3.2	333	36.3	656	11.1	− 2.5	− 16.2
H7 (Alradda)	Alluvial sediments	558938	2995755	32.8	22.02.2018	28.1	2.5	7.8	570	16.6	345	135.1	0.5	1.9	179	23.3	333	10.6	− 3.2	− 14.1
					22.11.2018	28.6	2.3	7.5	565	21.7	290	108.9	0.2	2.6	176	24.2	296	8.3		
H8 (Om Dalfa)	Basement rocks	556443	2986417	Spring	22.02.2018	20.4	2.1	8	448	0.8	375	82.8	1.6	2.2	166	5.3	305	10.6	− 5.0	− 30.7
					22.11.2018	22.0	2.2	7.8	517	2.4	351	56.9	1.9	3.1	169	5.1	309	9.8		
H9 (Om Dalfa)	Basement rocks	556342	2986401	Spring	22.02.2018	20.5	1.6	7.4	332	1.9	284	71.9	1.1	1.5	129	4.8	234	7.5	− 4.8	− 28.7

Table 1 (continued)

	Aquifer	X (UTM)	Y (UTM)	Well depth [m]	Sampling date	T [°C]	EC [mS/cm]	pH [-]	Cl [mg/l]	NO_3	SO_4	HCO_3	Br	F	Ca	Mg	Na	K	$\delta^{18}O$ [‰ SMOW]	δ^2H
H10 (Elojaira)	Basement rocks	565174	2990990	16.3	22.02.2018	20.6	7.8	8.5	2000	3.8	1370	82.8	4.4	0	152	153	1290	81.2	0.3	− 13.7
					22.11.2018	23.0	7.5	8.3	1900	2.4	1000	95.9	4	< 0.01	135	142	1310	79.8		
Coastal plain																				
P1	Limestone	564408	3027785	32	1.10.16	28	7.7	7.5	2700	3.5	1360	91.5	22.8	1.3	545	260	1080	33	− 6.2	− 49.3
P2	Limestone	564390	3028579	32	1.10.16	28.3	9.1	7.7	3240	2.3	1460	91.5	24	1.5	667	316	1230	17.7	− 5.9	− 47.6
P3	Limestone	563021	3026416	108	1.10.16	30	7.3	7.3	2390	8.3	1420	126.3	21.8	0.9	516	267	1020	18.8	− 5.6	− 49
P4	Limestone	561503	3028365	102	1.10.16	27.5	19.6	7.2	7700	9.6	2950	248.3	58.8	5.3	1160	751	2970	106	− 5.3	− 45.9
P5	Limestone	562249	3027242	69	1.10.16	37.9	7.4	7.6	2960	0.3	1400	117.6	25.2	1.2	552	260	1070	21.4	− 5.7	− 47.2
P6	Limestone	562920	3026885	108	1.10.16	30	12.1	7.2	4240	52.3	2530	91.5	33.3	1.3	916	441	1800	27.5	− 5.2	− 47.1
P7	Limestone	563255	3025987	86	1.10.16	31.4	7.3	7.3	2570	7.9	1320	117.6	25	0.5	534	247	1010	12.5	− 6.4	− 50.3
P8	Limestone	561188	3028523	108	1.10.16	31.7	8.9	7.4	2870	0.4	2650	119.8	27.2	3.7	852	371	1150	36.7	− 5.8	− 42
P9	Limestone	561725	3028212	75	1.10.16	36.4	14.2	7.1	5060	0.3	2590	117.6	39	3.5	1030	502	2190	89	− 5.9	− 48.3
Seawater Red Sea																				
S1	Red Sea water	573622	3034435		Oct. 2016		57.8	8.1	22,900	< 5	3100	176.9	78.3	5	392	1420	13,400	397	+2.3	+11.6

the Red Sea (S1) the water loss due to evaporation might be in a range of 40–50%, and the solution is concentrated by a factor 1.8–2.

Groundwater Groundwater samples can be differentiated in several groups:

1. Samples drop close to the LMWL:
   In the range of the actual precipitation data ($\delta^2H > -20$, $\delta^{18}O > -4$) Red Sea Hills group (red squares in Fig. 4a): samples H2, H3, H6, H7.
2. Samples drop on or close to the GMWL:
   Depleted in comparison to actual precipitation ($\delta^2H \approx -30$, $\delta^{18}O \approx -5$) Red Sea Hills group: samples H8, H9 at location Om Dalfa, H1 (δ^2H‰/$\delta^{18}O$‰: − 42.03/− 5.92) and coastal plain group, sample P8.
3. Samples with deviation from the LMWL and GMWL and stronger depletion in δ^2H and $\delta^{18}O$:
   a. Deep wells of coastal plain group (green squares in Fig. 4a); and from Red Sea Hills group: Wadi Melaha spring and stream (H4, H5: evaporated);
   b. Red Sea Hills, samples H10 (evaporated).

Samples of group 1 can be related to infiltration waters of modern precipitation under warm infiltration conditions.

Samples of group 2 are of intermediate waters that consist of different mixtures between water from group 1 and 3.

Samples of group 3 represent fossil groundwater with an increased depletion of the stable isotopes and a clear deviation from the LMWL.

Representing the relationship between ^2H and d-excess in Fig. 4b (excluding the evaporated samples H5 and H10) supports the separation of the three groups. The d-excess of group 1 is similar to this of the floodwater. Samples of group 2 plot on a line with H8 and H9 and the deep wells of group 3 seem to have differences in d-excess and indicate colder recharge conditions and more humidity.

Concentrations of selected major and trace elements

To follow the development of concentration which increases during the rainfall events, after reaching the ground surface and in the aquifers, Schoeller diagram was used for the four water groups in Fig. 5a.

The lowest concentrations are found in rainwater. The rainwater is dominated by Cl, SO_4, Na, and Ca in a range between 0.1 and ≈ 1 mmol/l. In areas close to the sea, the uptake of sea-spray is remarkable, shifting rainwater composition towards seawater. As shown in Sect. 4.2.1 by means of the stable isotopes, the sample R5 is evaporated and concentrated by a factor 1.5–2. In addition, other samples might be influenced by evaporation and are consequently concentrated

Table 2 ^{3}H, He isotopes and Ne data for groundwater from El Gouna Area

No Well/location	Well depth [m]	Groundwater depth [m]	Sampling date	Tritium (TU)	^{3}He [Nml/g]	^{4}He [Nml/g]	$^{3}He/^{4}He$	Ne [Nml/g]
P1	30	14.87	01-10-2016	< 0.03	$8.37.10^{-14}$	$1.77.10^{-07}$	$4.73.10^{-07}$	$1.69.10^{-07}$
P2	30	11.00	01-10-2016	< 0.03	$1.14.10^{-13}$	$3.28.10^{-07}$	$3.46.10^{-07}$	$1.66.10^{-07}$
P3	108	25.90	01-10-2016	< 0.03	$8.45.10^{-14}$	$1.69.10^{-07}$	$5.01.10^{-07}$	$1.68.10^{-07}$
P6	108		01-10-2016	< 0.03	$8.04.10^{-14}$	$1.06.10^{-07}$	$7.61.10^{-07}$	$1.83.10^{-07}$
P5	69		01-10-2016	< 0.03	$5.97.10^{-13}$	$2.92.10^{-06}$	$2.05.10^{-07}$	$1.67.10^{-07}$
P4	102	47.88	01-10-2016	< 0.03	$7.23.10^{-14}$	$1.32.10^{-07}$	$5.47.10^{-07}$	$1.65.10^{-07}$
P7	86		01-10-2016	< 0.03	$5.38.10^{-13}$	$2.10.10^{-06}$	$2.56.10^{-07}$	$1.73.10^{-07}$
H1	150	120	23-02-2019	< 0.6				
H2	–		23-02-2019	< 0.6				
H3	10		23-02-2019	< 0.6				
H6	10		22-11-2018	< 0.6				
H8	–		22-11-2018	< 0.4				
H10	15		22-11-2018	0.7 ± 0.4				

(e.g. R1, R4) and the concentration of the unevaporated rainwater is lower.

The floodwater samples have increased concentration compared to the rainwater samples. The dominating ions are Cl, SO_4, Na, and Ca in the range of ≈1–10 mmol/l. The distribution of the ions is relatively similar to the rainwater samples. These increased concentrations are related to evaporation and to the water/rocks interaction and the uptake of terrestrial salts resulting from variablbe rocks compositions which exist in the study area (eg. NaCl, $CaSO_4 \times 2H_2O$, $CaCO_3$).

Sample F7 (the only one with analyses of the stable isotopes) does not show evaporation effects (Sect. 4.2.1), therefore the concentration here is related only to the water/rocks interaction. The terrestrial chlorides and sulfates at the surface are the result of evaporating rainwater, and close to the coast of transported sea spray.

The samples from groundwater Red Sea Hills show a broader scattering of the concentrations. Samples of groups 1 are dominated by Cl, SO_4, Na, and Ca in a range of of ≈1 to ≈54 mmol/l. The elevated F concentration results from the uptake of apatite and fluorite which were detected in the XRD analysis. Deviations from the general pattern which characterizes this group can be observed in the concentrations of the evaporated samples (H5, H10) in Wadi Melaha spring and Elojaira well (H10) and the samples belong to H1, H4. H1 and H4 samples show comparable concentrations to the coastal plain group with elevated concentrations in all ions. Their concentrations of Br and F are similarly elevated as in the coastal plain group and confirm that these samples are probably mixed with water from the deep wells.

Piper diagram in Fig. 5b was used to represent the distribution of groundwater groups. HCO_3 and Cl positions in the diagram were exchanged for a better representation. While the coastal plain group shows a tendency of increasing salinity, the Red Sea Hills samples are very scattered indicating the different lithologies of the hosting rocks. The ratios of SO4/Cl and (Ca + Mg)/(Na + K) indicate two subgroups in the coastal plain group (Jahnke et al. 2019). The distribution pattern confirms that seawater and the coastal plain group are not in hydraulic connection despite of the intensive pumping in this area. The different Br/Cl ratios (Edmunds 1996) between this group ($3.3–4.3 \times 10^{-3}$) and seawater ($1.4–1.55 \times 10^{-3}$) indicate as well that no mixing with seawater take place in these wells (Jahnke et al. 2019).

To quantify the chemical development from rain to flood and groundwater averages of the parameters of the hydrochemical groups were calculated (based on logarithmic values). The balanced changes of the averaged concentrations from rainwater to the other groups are shown in Fig. 6.

From rainwater to floodwater, an averaged increase occurs of the concentrations of Cl, SO_4, Na, and Ca of around 3–3.5 mmol/l, for K and Mg of ca. 0.3 and 0.6 mmol/l, respectively. No significant increase can be detected for Br and F. The concentration differences are small and might be related to the strong scattering and the sparse data in both groups. The flood water samples were collected during or shortly after the precipitation events, so that evaporation play only a minor role and the increase in the concentrations is related to an uptake of terrestrial salt, dust and sea spray (all flood water samples were taken relatively close to the coast in distances 5–10 km). The development is dominated by an uptake of ca. 3 mmol/l NaCl and $CaSO_4$ (gypsum) and carbonate minerals (calcite, dolomite).

The waters of the Red Sea Hill group show the same tendencies as floodwater for Ca, Mg, K, and SO_4. The average concentrations of Cl and Na are increased by 15 ca. mmol/l compared to rainwater and 12 mmol/l compared to the flood

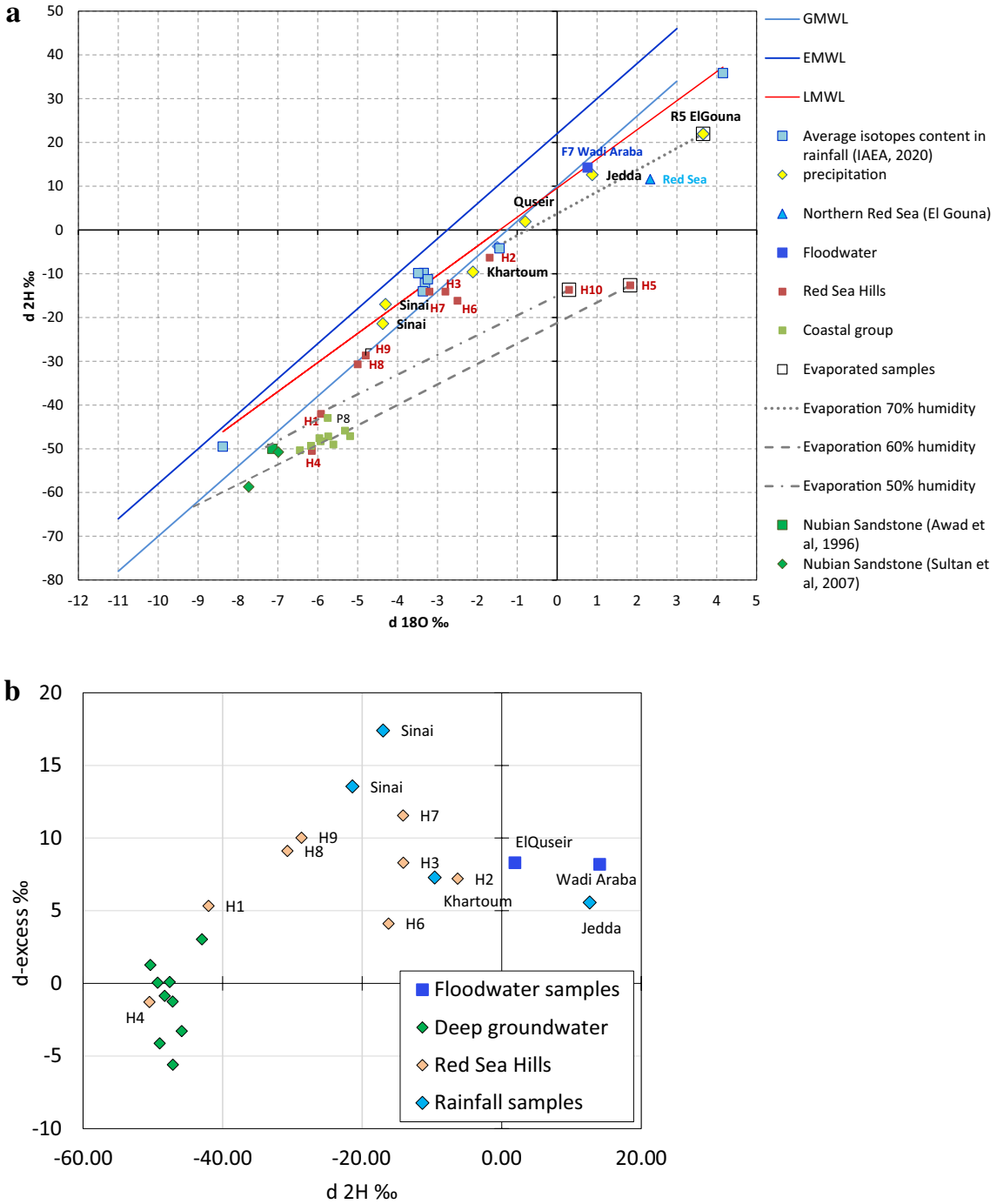

Fig. 4 **a** ^{18}O-2H diagram for precipitation and groundwater in the investigated area **b** d-excess-δ^2H relationship in floodwater, Red Sea Hills group and the coastal plain group

water. In addition, a small but detectable increase of Br and F occurs. Based on the hydrochemical results, the groundwater of the Red Sea Hills seems to be an infiltrated flood water with an additional uptake of NaCl (mixing with NaCl-rich solutions or solution of NaCl).

Tritium/^{3}Helium/^{4}Helium

The ^{3}H content and the concentrations of Helium isotopes ^{3}He and ^{4}He, Ne and the ratio ^{3}He/^{4}He are listed in Table 2. In the Red Sea Hills group, ^{3}H could be detected only in H10 in Elojaira and the rest shows activity < 0.55 TU indicating

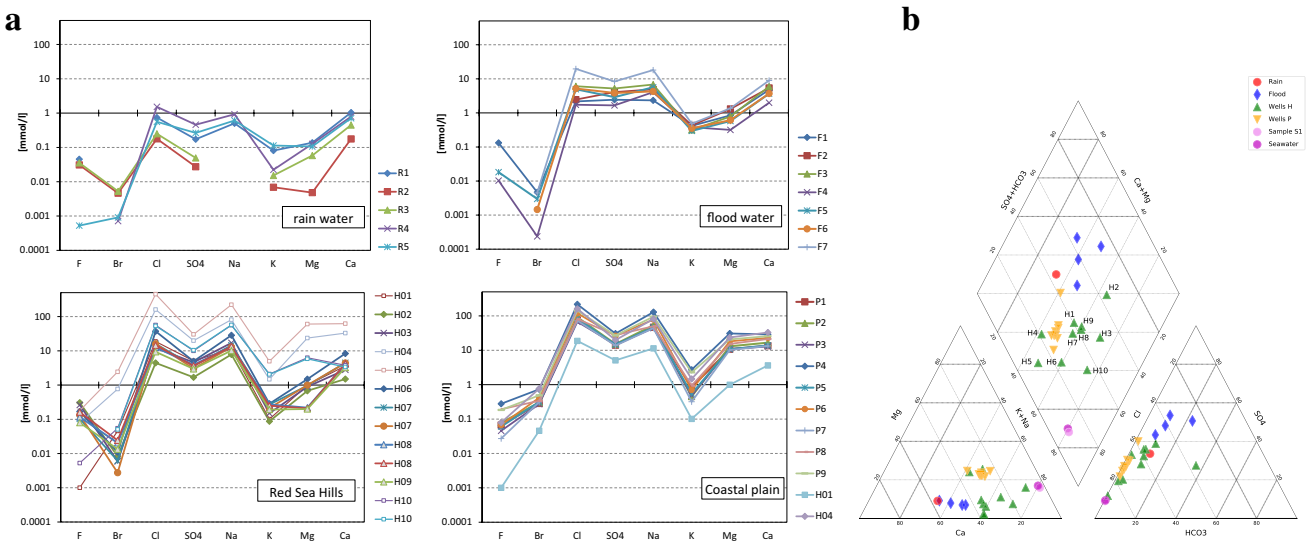

Fig. 5 **a** Schoeller plots of the hydrochemical analysis of rainfall samples, flood samples, Red Sea Hills samples and the coastal plain samples. **b** Modified Piper plot with the compositions of the different hydrochemical groups in the investigation area

that water has not been recharged since 1955. H10 is an open well in the basement and ^{3}H of 0.7 TU has been detected. This sample as it was mentioned reflects a strong evaporation effect and the well is not protected and has a diameter of 3.5 m. Since ^{3}H can enter the aquifer only via rain or flood events, the well might have received rain or floodwater through the flash floods events and this can be the reason behind the detection of ^{3}H. The activity of ^{3}H in all wells of the coastal plain group is less than the detection limit 0.03 TU meaning the component of He_{trit} (Fontes 1983; Lucas and Unterwegers 2000) does not exist in the total ^{3}He (Poreda et al. 1988). The absence of this component leads to the conclusion that the existing of terrigenic He is a result of U and Th decay in the earth crust and earth mantle (Schlosser et al. 1989). The atmospheric ratio symbolized as

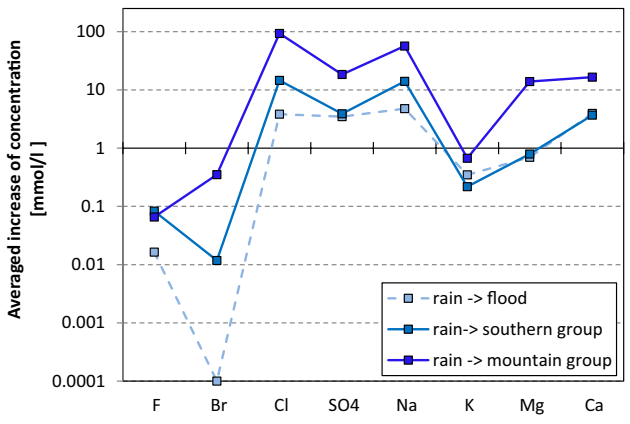

Fig. 6 Averaged hydrochemical development and increase of mineralization from rainwater to floodwater and the different groundwater groups red Sea Hills without evaprated samples (H5, H10)

*R*a is equal to $(1.384 \pm 0.006)0.10^{-6}$ (Clarke et al. 1976). The ^{3}He/^{4}He ratio of crustal helium is in a range from 1.10^{-8} to 3.10^{-8} corresponding to $\approx 0.01R$a (Mamyrin and Tolstikhin 1984) and the upper mantle is characterised by a ^{3}He/^{4}He ratio of $\approx 10^{-5}$ or $\approx 8R$a (Graham 2002; Kaudse, 2014). By the application of this ratios, the separation of Helium components into crustal He and mantle He is possible as presented by Aeschbach-Hertig (2005) (Sect. 3.2.2). The ratios ^{3}He/^{4}He and Ne/He were calculated for each sampled location (Table 2). The ratio ^{3}He/^{4}He ranges between 0.15 Ra in well P5 and 0.5 *R*a in P6 and consequently higher than the typical crust ratio $\approx 0.01R$a indicating a contribution from the mantle. The mixing between terrigenic He components in groundwater is illustrated in Fig. 7. In the case of pure mixture of radiogenic and mantle He and absence of He_{trit}, the samples will drop between the radiogenic line and the mantle line. Because of their higher ^{3}He/^{4}He rather than the radiogenic line, the samples from the deep wells in the coastal plain group drop over the radiogenic helium line and indicate consequently a contribution of He from the mantle. Applying the approach suggested by Aeschbach-Hertig (2005), the He mantle was calculated with a value around 2% in all samples.

The concentrations of Li which may play a role in elevating the radiogenic He ratio range in the coastal plain group range between 0.05 and 0.35 mg/l. No real correlation can be recognised between the ^{3}He/^{4}He ratio and the Li concentrations (Fig. 8). The two samples H6, H7 which belong to dug wells exist in the loose sediments of the Wadis deposits have Li concentrations of 0.2–0.3 mg/l. The high Li values in the groundwater of the Wadi sediments depend on the weathering results of the basement rocks and due to the

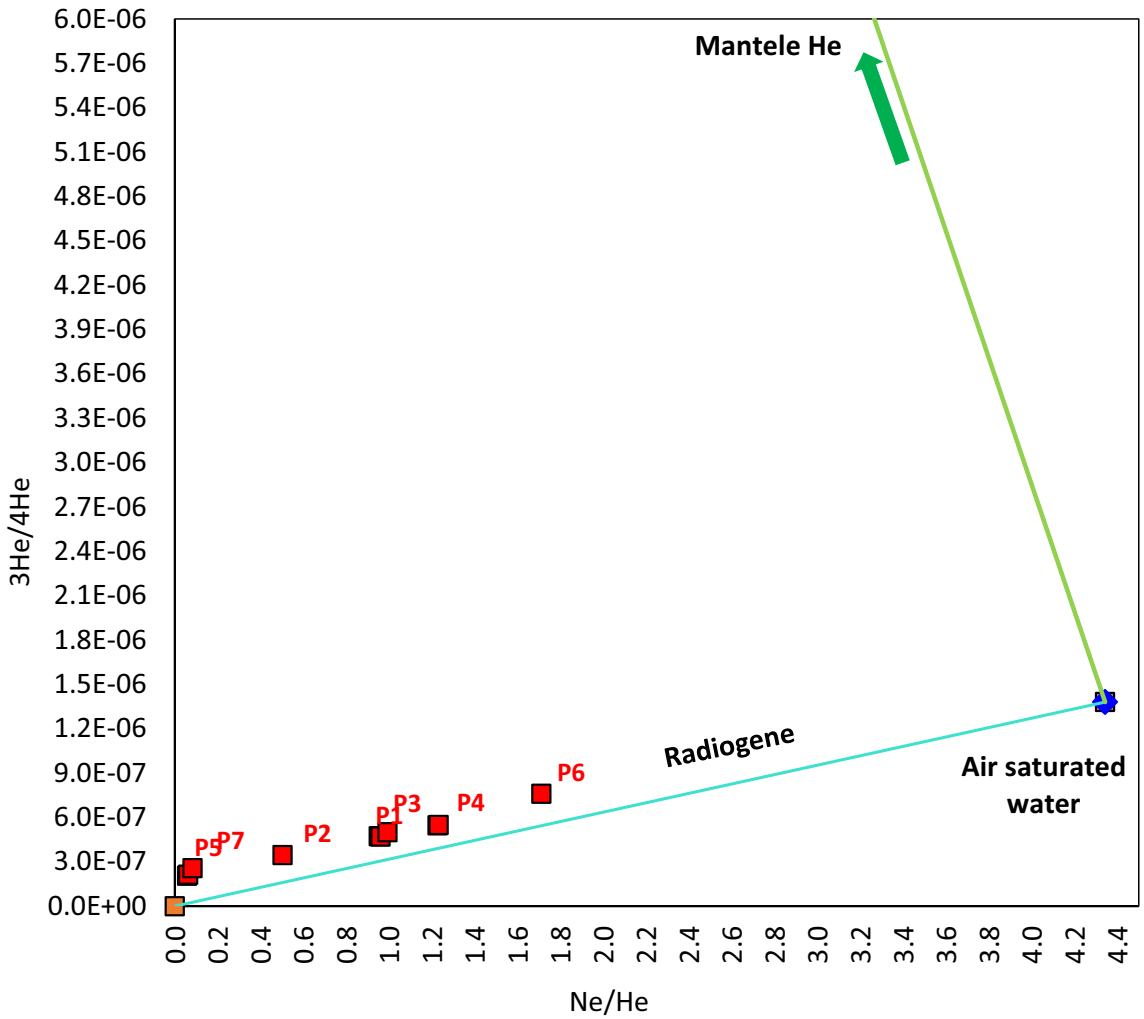

Fig. 7 $^{3}He/^{4}He$ vs Ne/He in the water samples of the coastal plain group listed in Table 2. The components of the atmospheric He, crust and mantle He are demonstrated on the graph. The Ne/He for the atmosphere is 4.34 and $^{3}He/^{4}He$ value is of 1.38E-06

higher contact surface in the porous sediments rather than in the basement fractures, similar concentrations of Li in these wells are expected.

Noble gas equilibrium temperatures

Unlike the He concentrations in groundwater, the Ne concentrations do not increase in groundwater therefore it can used as a tracer to reconstruct the conditions (T, P) in the catchment area. The catchment area of the coastal plain group aquifer is not known and since the ^{3}H was not detected in this water, the flow path of the groundwater should be far from the recharge place or the residence time of groundwater in the underground is very long. In both cases, the altitude and the temperature of the rainfall are not known; therefore, a wide margin for altitude of 50–500 m.a.s.l and for temperature 5–30 °C was chosen to calculate the infiltration

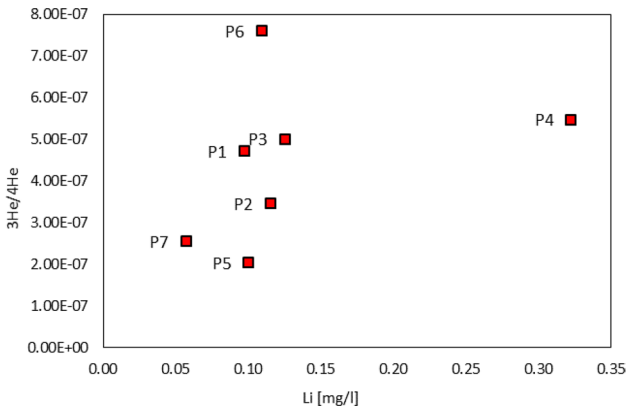

Fig. 8 Li–$^{3}H/^{4}He$ concentrations in the samples of the coastal plain group

temperature and the altitude of the recharge for the samples of this group (Fig. 9).

The equilibrium temperature which was simulated assuming that the infiltration altitude is 500 m.a.s.l is between 13 and 30 °C indicating a wide range and less plausibility. 13 °C would go consistently with the temperatures calculated from the stable isotopes condensation conditions. 25–30 seems to be very warm for the infiltration conditions which were assumed for the rainy period in Egypt (Thorweihe 1982; Schneider 1986; Awad et al. 1996). For an equilibrium infiltration temperature of 20 °C, the topographic altitude would be in a range between 100 and 1000 m.a.s.l.

Since only He and Ne were measured in this study, the reconstruction of the paleoclimate data requires the application of more noble gases where the influence of the excess air can be compensated through the number of the measured noble gases. The studies which have been applied in this appraoch resulted higher temperatures than given from the ^{18}O and ^{2}H. Even having data from all noble gases analysed (Beyerle et al. 2002; Lavastre et al. 2010; Lehmann et al. 2003; Pinti et al. 1997), this method seems not to be reliable dealing with fossil water. Even for younger water, the method lacks of evidence compared with classical stable isotopes. Temperature diffrences of five degrees were mentioned in several studies (Andrews and Lee 1979; Beyerle et al. 1998).

Discussion

Following the marine-atmosphere isotope model of Craig and Gordon (1965), a Raleigh distillation at 75% relative humidity of the northern Red Sea would result in vapor of the homogenous layer with δ^{18}O and δ^{2}H values of approximately − 11 and − 80‰, respectively. Precipitation formed from this vapor has isotope values of δ^{18}O: − 2‰ and δ^{2}H: − 10‰. Rainout depletes the vapor and at 50% relative humidity the isotope values in the cloud layer would be δ^{18}O‰/δ^{2}H‰: − 15 and − 118‰. The determined isotope values of the precipitation fit well to the precipitation data and data of the groundwater group 1 (Sect. 4.2.1 groundwater) in Fig. 4a. Hence the northern Red Sea is most likely the main reservoir for vapor formation and precipitation in the research area.

The Red Sea water shows a deviation from the SMOW (Table 1: S1: δ^{18}O: 2.3‰; δ^{2}H: 11.6‰), which is typical for the northern part of the Red Sea, compare e.g. (Andrié and Merlivat 1989), (Table 1, Sect. 4.2.1, the northern red Sea). The concentrations of the conservative parameters Cl and Br are increased by factor of ≈1.14 comparing to standard seawater, so the loss of water by evaporation is ≈13%. A linear correlation exists between salinity and ^{18}O and δ^{2}H so the enrichment is related to evaporation processes (Andrié and Merlivat 1989). The slope δ^{2}H /δ^{18}O to the SMOW is 4.99 what can be related to a humidity of 70%, is reliable for an evaporation process above the open Sea.

The mean weighted local precipitation (δ^{18}O‰/δ^{2}H‰: − 0.3/7) taken from the LMWL-GMWL intersection is

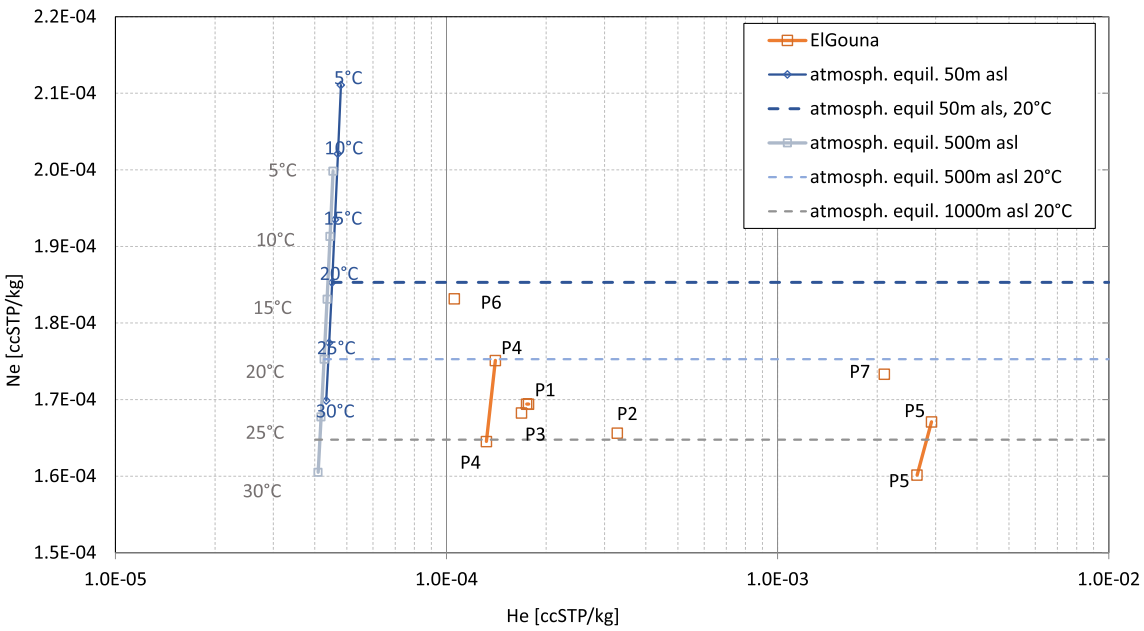

Fig. 9 Estimation of equilibrium pressure and temperature in groundwater samples of the coastal plain

enriched in comparison to values from the theoretical determined precipitation after Craig and Gordon (1965). The deviation between the two indicates that sub-cloud evaporation of falling raindrops that enriches the precipitation falling to the ground, play a role.

Mixtures of groundwater of group 1 and 2 (Sect. 4.2.1, groundwater) are not necessarily obvious. The springs of Om Dalfa (Sample H8 and H9) lie within the basement rock of the Red Sea Hills. The isotope values of these springs are depleted in comparison to values of sample H2 that is also situated in the basement rock. An explanation of this deviation was brought up by Sultan et al. (2011) who found depleted groundwaters within subsided blocks that connected aquifers bearing fossil and modern groundwaters in a research area north west of of El Gouna. In Fig. 4a, sample H1 and P8 deviate from the position of the fossil groundwater from group 3 (Sect. 4.2.1, groundwater). The trend towards the LMWL and the minor deviation in $\delta^{18}O$ and $\delta^{2}H$ compared to the fossil groundwaters imply a minor influence from modern groundwaters. The spring of Melaha (Sample H4) plot within the fossil groundwaters of group 3 of the deep wells (see Fig. 4a). Despite its location near by the Red Sea it is neither influenced by modern groundwaters nor by seawater intrusion since this would result in enriched isotope values. Evaporation of the emerging water from the Melaha spring produces enriched stream water (Sample H5). Interpolation of a evaporation line with 60% relative humidity connects sample H4 with sample H5 in Fig. 4a confirming the direct link between the two.

The coastal plain group wells show a different chemical evolution pattern and different groundwater temperatures. The group itself shows in Fig. 5b differences in the concentrations between the northern part and the southern part along the short distance (Jahnke et al. 2019). The EC value decreases from well P4 (19.6 mS/cm) to well P7 (7 mS/cm). The higher salinity in the northern wells can be explained through the possible mixing with the spring water (sample H4). The fault system seems to have different hydraulic conductivities along the locations of the wells. The less hydraulic conductivity is evident with the lower yield of the northern wells in the coastal plain. The lower salinity in the southern wells can be explained with a better conductivity of the faults linking the deep depressions SW of Abu Shaar as proven by Sultan et al. (2011). It is to expect that no seawater intrusion influences the deep wells because of the barrier function of the faults along the Red Sea margin. As long as a gradient exists in the groundwater table between the deep wells and the big sediment accumulations in Wadi El Melaha, the deep wells will be supplied.

Winckler et al (2001) investigated three deep brine locations at different depths along the Red Sea: the young southern spreading part known as Discovery Deep (Cochran et al. 1986), the central transition part or Atlantis II Deep and the northern part or Kebrit Deep. The three deeps are located at a distance of around 450 km. The investigated area is west to the Kebrit Deep which is located between 23°20′ N and 29°57′ N and represents the pre stage of seafloor spreading in development of the continental margin (Bonatti 1985; Winckler et al. 2001). The mantle He contribution with 9% in Kebrit deep brine accumulates according to Winckler et al. (2001) migrates from deeper sedimentary or crustal horizons. The Ra for this brine has values in the range between $1.06.10^{-6}$ and $1.69.10^{-6}$. In contrast to the spreading zones in the centre of the Red Sea Graben system, the strike slip fault of its shoulder west of Hurghada has a much lower permeability because it is under pressure. Consequently, the amount of He from the mantle may not exceed the analysed 2%.

Figure 10 shows the Abu Shaar Fault which runs parallel to the deep wells in the coastal plain group. The block east of the fault is part of the Red Sea Graben system and slipped some hundred meters down. Due to the pressure the fault is a barrier and the groundwater flowing from east to west following the morphological gradient is rising up along the fault. Sea water intrusion in wells east of the fault would be difficult. West of Abu Shaar mountains, the NNW striking Wadi Melah extending 60 km to the north and ending south of Abu Shaar takes place and it could be the main area for inflow. An oasis did exist in former time in front of Abu Shaar Mountain with a captured spring (Bir Abu Shaar) described and shown on a picture (Fig. 2; Madgwick et al. 2016). The fault continues southward and run off from the Red Sea hills recharges the porous aquifers west of the fault mainly at the mountain foot from a 7–8 years precipitation event. The recharge for the shallow wells seems to be dependent on rising groundwater too, as it cannot pass the impermeable barrier.

Conclusion

The main concluding remarks are as follows:

The collected floodwater in the area is mainly influenced by the rainwater/rock interaction and reflects the variability of rocks in the region which influence concentrations of the sampled water.

^{3}H activity at all sampled locations is under the detection limit. The stable isotopes and hydrochemical parameters confirm that groundwater in the region is either recharged from modern precipitation, a mixture of groundwater recharged by modern precipitation and fossil groundwater or fossil groundwater.

The deep wells of the coastal plain group with elevated temperatures up to 38 °C show a higher geothermal gradient at the fault zone of Abu Shaar Plateau. The magmatic

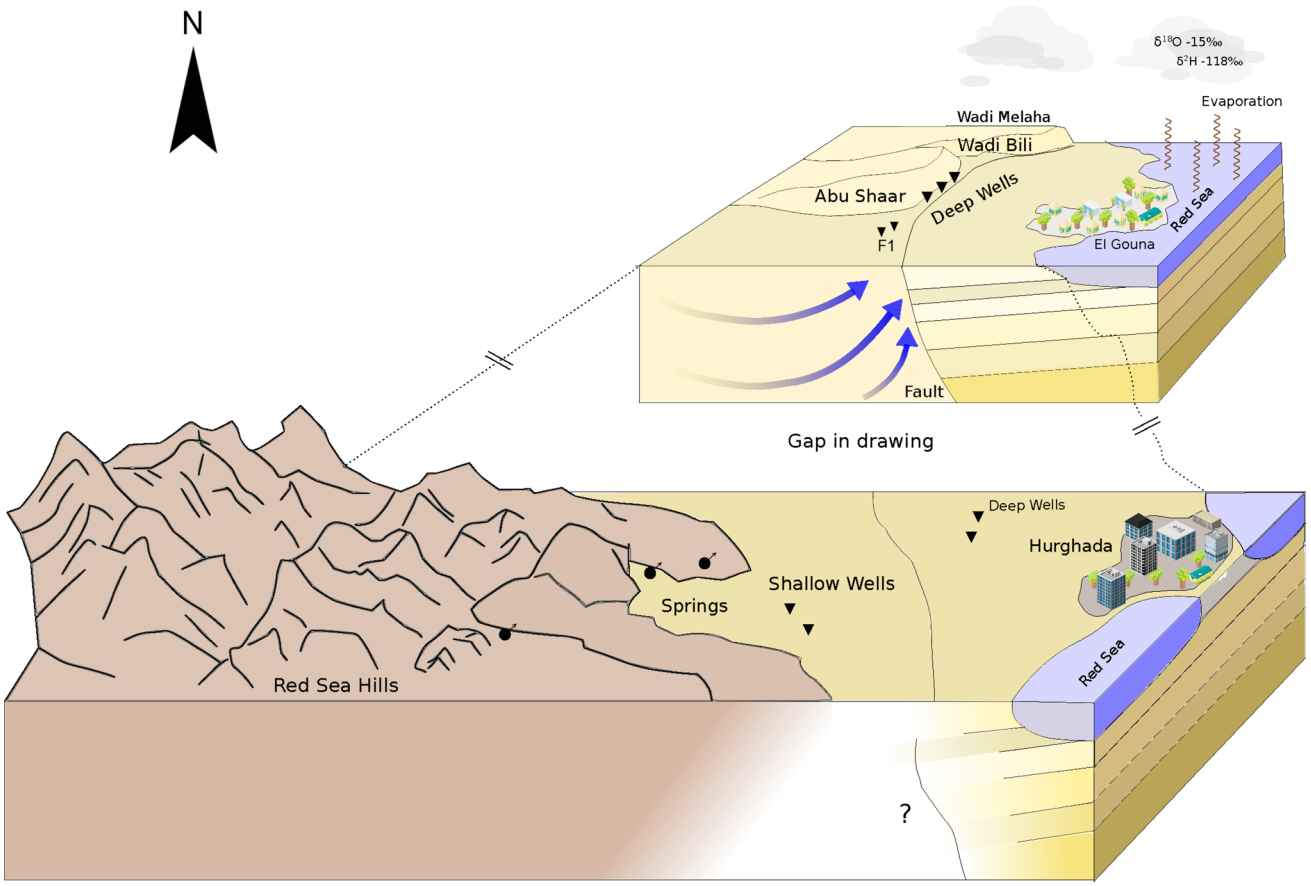

Fig. 10 3D schematic conceptual model showing sampling points in the area

He ratio of 2% confirms that the fault at the sampled wells transports deep hot water to the aquifer.

There is no evidence for marine water intrusion in all deep wells west of the Red Sea which are located parallel to the fault along Abu Shaar Plateau and further south. This confirms the role of the fault at this location as a barrier against the ingress of seawater from the Red Sea. Further research may more precisely delineate more precise the recharge areas and help understand the groundwater flow pathways in determining their age.

Acknowledgments The authors would like to thank Mr. Hilal and Mr. Zaki from the water authority in El Gouna for facilitating the sampling of the deep wells in the farm and Mr. Askar for the initial sampling in 2014. Mr. Bollkemper and Mr. Tzoupanos are highly acknowledged for their support in the lab. Thanks go to the anonymous reviewers who took the time to read and review this article.

Funding Open Access funding enabled and organized by Projekt DEAL. All external analyzing expenses were paid by the central institute El Gouna-Technische Universität Berlin.

Data availability All data used in this manuscript are available.

Compliance with ethical standards

Conflict of interest The authors confirm that there are no known conflicts of interest associated with this publication.

References

Abdel Samie S, El-Sadek M (2001) Groundwater recharge and flow in the Lower Cretaceous Nubian Sandstone aquifer in the Sinai Peninsula, using isotopic techniques and hydrochemistry. Hydrogeol J 9:378–389. https://doi.org/10.1007/s100400100140

Aeschbach-Hertig W (2005) A comment on "Helium sources in passive margin aquifers—new evidence for a significant mantle 3He

source in aquifers with unexpectedly low in situ 3He/4He production. Earth Planet SciLett 240:827–829
Aeschbach-Hertig W, Peeters F, Beyerle U, Kipfer R (1999) Interpretation of dissolved atmospheric noble gases in natural waters. Water Resour Res 35:2779–2792
Aeschbach-Hertig W, El Gamal H, Dahab KA, Kipfer R (2006) Environmental tracer study of groundwater recharge near the Nile Delta, Egypt. Determining paleotemperature and other variables by using an error-weighted, nonlinear inversion of noble gas concentrations in water. GeochimCosmochimActa 63:2315–2336
Alsharhan A (2003) Petroleum geology and potential hydrocarbon plays in the Gulf of Suez rift basin, Egypt. AAPG Bull 87(1):143–180
Andrié C, Merlivat L (1989) Contribution des données isotopiques de deutérium, oxygène-18, hélium-3 et tritium, à l'étude de la circulation de la Mer Rouge. Oceanologica Acta 12(3)
Andrews JN, Lee DJ (1979) Inert gases in groundwater from the bunter sandstone of England as indicators of age and paleoclimatic trends. J Hydrol 41:233–252
Askar A (2014) Groundwater chemistry and geology of the unconfined aquifer of the region west of El Gouna—Egypt: unpublished. Master thesis, Technische Universität Berlin
Awad MA, Hamza MS, Atwa SM, Sallouma MK (1996) Isotopic and hydrogeochemical evaluation of groundwater at Qusier-Safaga area, eastern desert, Egypt. Environ Geochem Health 18:47–54
Bath AH, Edmunds WM, Andrews JN (eds) (1979) Paleoclimatic trends deduced from the hydrochemistry of Triassic sandstone aquifer. International Atomic Energy Agency (IAEA), United Kingdom
Beyerle U, Purtschert R, Aeschbach-Hertig W, Imboden DM, Loosli HH, Wieler R, Kipfer R (1998) Climate and groundwater recharge during the last glaciation in an ice-covered region. Science 282:731–734. https://doi.org/10.1126/science.282.5389.731
Beyerle U, Aeschbach-Hertig W, Peeters F, Kipfer R, Purtschert R, Lehmann B, Loosli HH, Love (2002) Noble gas data from the Great Artesian Basin provide atemperature record of Australia on time scales of 10^5 years, Research collection, ETH Zürich, report. https://doi.org/10.3929/ethz-a-004301675
Biggs BG, Rohling EJ (2000) An oxygen isotope data set for marine waters. J Geophys Res 105(C4):8527–8535
Bonatti E (1985) Punctiform initiation of sea£oor spreading in the Red Sea during transition from a continental to an oceanic rift. Nature 316:33–37
Bosworth W, McClay K (2001) Structural and stratigraphic evolution of the Gulf of Suez Rift, Egypt: a synthesis. In: Ziegler PA, Cavazza W, Robberston AHF, Crasquin-Soleau S (eds) Peri-Tethys Memoir 6: Peri-Tethyan Rift/Wrench Basins and Passive Margins. Paris (ISBN 2-85653-528-3) (Mem Mus Natn Hist Nat 186:567–606)
Bosworth W, Taviani M (1996) Late Quaternary reorientation of stress field and extension direction in the southern Gulf of Suez, Egypt: Evidence from uplifted coral terraces, mesoscopic fault arrays, and borehole breakouts. Tectonics 15:791–802. https://doi.org/10.1029/95TC03851
Bosworth W, Huchon P, McClay K (2005) The Red Sea and Gulf of Aden Basins. J Afr Earth Sc 43:334–378. https://doi.org/10.1016/j.jafrearsci.2005.07.020
Bowen GJ, Putman A, Brooks JR, Bowling DR, Oerter EJ, Good SP (2018) Inferring the source of evaporated waters using stable H and O isotopes. Oecologia 187(4):1025–1039. https://doi.org/10.1007/s00442-018-4192-5
Castro MC (2004) Helium sources in passive margin aqui- fers: new evidence for a significant mantle 3 He source in aquifers with unexpectedly low in situ3He/4He production. Earth Planet SciLett 3–4:897–913
Clarke WB, Jenkins WJ, Top Z (1976) Determination of tritium by mass spectrometric measurement of 3He. Int J ApplRadiatIsot 27:515–522. https://doi.org/10.1016/0020-708X(76)90082-X
Cochran JR, Martinez F, Steckler MS, Hobart MA (1986) Conrad deep: a new northern Red Sea deep. Origion and implications for continental rifting. Earth Planet SciLett 78:18–32
Craig H, Gordon L I, (1965) Deuterium and oxygen-18 variations in the ocean and the mairitme atmosphere. In: Paper presented at the Stable Isotopes in Oceanographic Studies and Paleotemperatures, Spoleto, Italy
Dansgaard W (1964) Stable isotopes in precipitation. Tellus XVI:436–468. https://doi.org/10.1111/j.2153-3490.1964.tb00181.x
Edmunds M (1996) Bromine geochemistry of British groundwaters. Mineral Mag 60:275–284
Eissa MA, Thomas JM, Pohll G, Hershey RL, Dahab KA, Dawoud MI, ElShiekh A, Gomaa MA (2013) Groundwater resource sustainability in the WadiWatir delta, Gulf of Aqaba, Sinai, Egypt. Hydrogeol J 21:1833–1851. https://doi.org/10.1007/s10040-013-1031-y
El-Sadek M, Tantawi MA, Salem WM (1998) Recharging mechanisims and salinization trends of the groundwater resources in Hurghada Area, Egypt: Environmantal and geochemical approach. El Minia Science Bulletin 11 (part 1), El Minia University, Faculty of Science, Geology section, ISSN 1110/2454
Fontes J (1983) Dating of groundwater, guidebook on nuclear technique In: Technical report series no 91. IAEA, Vienna
Klump S, Brennwald MS, Kipfer R (2006) Comment on "Noble gases and stable isotopes in shallow aquifer in southern Michigan: implications for noble gas paleotemperature reconstruction for cool climates" by Chris M. Hall et al. Geophys Res Lett. https://doi.org/10.1029/2006GL027496
Gat JR, Carmi I (1970) Evolution of the isotopic composition of atmospheric waters in the Mediterranean Sea area. J Geophys Res 75:3039–3048. https://doi.org/10.1029/JC075i015p03039
Gibson JJ, Edwards TWD, Bursey GG (1993) Estimating evaporation using stable isotopes. Nord Hydrol 24:79–94
Gonfiantini R (1986) Environmental Isotopes in lake studies, The Terrestrial environment B. In: Fritz P, Fontes J (eds) Environmental isotopes in lake studies, Handbook of environmental isotope geochemistry. Elsevier, Amsterdam, pp 113–168
Graham DW (2002) Noble gas isotope geochemistry of mid-ocean ridge and ocean island basalts: characterization of mantle source reservoirs. Rev Mineral Geochem 47:247–317. https://doi.org/10.2138/rmg.2002.47.8
Greilling RO, El Ramly MF, Akhal HE, Stern RJ (1988) Tectonic evolution of the northwestern Red Sea margin as related to basement structure. Tectonophysics 153:179–191
Gupta P, Noone D, Galewsky J, Sweeney C, Vaughn BH (2009) Demonstration of high-precision continuous measurements of water vapor isotopologues in laboratory and remote field deployments using wavelength-scanned cavity ring-down spectroscopy (WS-CRDS) technology. Rapid Commun Mass Spectrom 23:2534–2542. https://doi.org/10.1002/rcm.4100
Hadidi A (2016) Wadi Bili: Example for Flash Floods in Wadis in the Eastern Desert of Egypt. A Structural Model for Evaluation of the Groundwater and Artificial Recharge. Doctoral Thesis, Technische Universität Berlin
Hefny K, Farid MS, Hussein M (1992) Groundwater assessment in Egypt. Int J Water Resour Dev 8:126–134
IAEA (1992) Statistical treatment of data on environmental isotopes in precipitation. Technical reports series, no 331. IARC, Vienna (revision edn)
IAEA (2009) Sampling Procedures for Isotope Hydrology. http://www-naweb.iaea.org/napc/ih/documents/other/Sampling%20booklet%20web.pdf
IAEA (2019) Global Network of Isotopes in Precipitation (GNIP)

Jahnke C, Wannous M, Troeger U, Falk M, Struck U (2019) Impact of seawater intrusion and disposal of desalinization brines on groundwater quality in El Gouna, Egypt, Red Sea Area. Process analyses by means of chemical and isotopic signatures. Appl Geochem 100:64–76

Kaudse T (2014) Noble gases in groundwater of the Azraq Oasis, Jordan, and along the central Dead Sea Transform,Two case studies. Doctoral Thesis, Combined Faculties for the Natural Sciences and for Mathematics

Kipfer R, Aeschbach-Hertig W, Peeters F, Stute M (2002) Noble gases in lakes and ground waters. Rev Mineral Geochem 47(1):615–700. https://doi.org/10.2138/rmg.2002.47.14

Kleinendorst T (2004) Water management in El Gouna. Technical report, reference, 9M7530.AO/R00002ffhKINijm

Klitzsch E, Linke HW (1983) Photogeologicalinterpritation map. Conoco, Coral Inc., Cairo

Kürten B, Zarokanellos ND, Devassy RP, El-Sherbiny MM, Struck U, Capone DG, Schulz IK, Al-Aidaroos IX, Jones BH (2019) Seasonal modulation of mesoscale processes alters nutrient availability and plankton communities in the Red Sea. ProgOceanogr 173:238–255

Lavastre V, La Salle C, Michelot J, Giannesini S, Benedetti L, Lancelot J, Lavielle B, Massault M, Thomas B, Gilabert E, Bourlès D, Clauer N, Agrinier P (2010) Establishing constraints on groundwater ages with Cl-36, C-14, H-3, and noble gases: a case study in the eastern Paris basin, France. ApplGeochem 25:1092–1093. https://doi.org/10.1016/j.apgeochem.2010.03.007

Lehmann B, Love A, Purtschert R, Collon P, Lossli HH, Kutschera W, Beyerle U, Aeschbach-Hertig W, Kipfer R, Frape SK, Herczeg A, Moran J, Toltikhin IN, Gröning M (2003) A comparison of groundwater dating with 81Kr, 36Cl and 4He in four wells of the Great Artesian Basin, Australia. Earth Planet SciLett 211:237–250

Linke HW (1986) Golf von Suez - Geologie und Tektonik. Doctoral Thesis, Technische Universität Berlin

Lucas LL, Unterweger MP (2000) Comprehensive review and critical evaluation of the half-life of tritium. J Res NatlInst Stand Technol 105:541–549

Madgwick TG, Moon FW, Sadek HS (2016) Preliminary geological report on the Abu Shaar el Qibli (Black Hill) district. Papeback reproduction of the original text from 1920. Wentworth Press, pp 24 (ISBN-13: 978-1374464490)

Mamyrin BA, Tolstikhin IN (1984) Helium isotopes in nature. Elsevier, Amsterdam

Margat J, Foster S, Droubi A (2006) Concept and importance of non-renewable resources In: Foster S, Loucks DP (eds) Non-renewable groundwater resources: a guide-book on socially-sustainable management for water-policy makers. IHP-VI, Series on Groundwater, No 10. UNESCO, Paris

Nada AA, Hussein MF, Awad MA, Salem WM (1996) Environmental isotopes and geochemistry of groundwater in the Red Sea Governerate of Egypt. IsotRadiat Res 28:33–42

Ozima M, Podosek FA (1983) Noble Gas Geochemistry. Cambridge Univ. Press, Cambridge, London, New York

Pfahl S, Sodemann M (2014) What controls deuterium excess in global precipitation? Clim Past 10:771–781

Pinti DL, Marty B, Andrews JN (1997) Atmosphere-derived noble gas evidence for the preservation of ancient waters in sedimentary basins. Geology 25:111. https://doi.org/10.1130/0091-7613(1997)025%3c0111:ADNGEF%3e2.3.CO;2

Poreda RJ, Cerling TE, Sallouma DK (1988) Tritium and helium isotopes as hedrologictraceres in a shallow unconfined aquifer. J Hydrol 103:1–9

Saber M, Abdrabo KI, Habiba OM, Kantosh SA, Sumi T (2020) Impacts of triple factors on flash flood vulnerability in Egypt: urban growth, extreme climate, and mismanagement. Geosciences 10:24. https://doi.org/10.3390/geosciences10010024

Salah G, Alsharhan AS (1996) Structural influence on hydrocarbon entrapment in the Northwestern Red Sea, Egypt. AAPG Bull 80:101–118

Schlosser P, Stute M, Sonntag C, Munnich KO (1989) Tritogenic 3He in shallow groundwater. Earth Planet SciLett 94:245–256

Schneider M (1986) Hydrogelogie des NubischenAquifersystems am Südrand des Dakhla-Beckens, Südägypten/Nordsudan, Reihe A/Band 71. Verlag von Dietrich Reimer, Berlin

Schmidt GA, Bigg GR, Rohling EJ (1999) Global seawater Oxygen-18 database - v1.22. https://data.giss.nasa.gov/o18data/

Stern RJ, Hedge CE (1985) Geochronologic and isotopic constraints on late Precambrian crustal evolution in the Eastern Desert of Egypt. Am J Sci 285:97–127. https://doi.org/10.2475/ajs.285.2.97

Sturchio NC, Arehart GB, Sultan M, Sano Y, Abokamar Y, Sayed M (1996) Composition and origion of thermal waters in the Gulf of Suez area, Egypt. ApplGeochem 11:471–479

Sturchio NC, Du X, Purtschert R, Lehmann B, Sultan M, Patterson J, Lu Z-T, Müller P, Bigler K, O'Connor TP, Young L, Lorenzo R, Becker R, El Alfy Z, El Kaliouby B, Dawood Y, Abdalla A (2004) One million year old groundwater in the Sahara revealed by krypton-81 and chlorine-3. Geophys Res Lett 31:L05503. https://doi.org/10.1029/2003GL019234

Sultan M, Yan E, Sturchio NC, Wagdy A, Abdel Gelil K, Becker R, Manocha N, Milewski A (2007) Natural recharge: a key to sustainable utilization of fossil groundwater. J Hydrol 335:25–36

Sultan M, Yousef AF, Metwall SE, Milewski A, Sauck W, Sturchio NC, Mohamed AMM, Wagdy A, El Alfy Z, Soliman F, Rashed M, Becker D, Sagintayev Z, Ahmed M, Welton B (2011) Red Sea rifting controls on aquifer distribution: constraints from geochemical, geophysical, and remote sensing data. GSA Bull 123:911–924

Sultenfuss J, Roether W, Rhein M (2009) The Bremen mass spectrometric facility for the measurement of helium isotopes, neon, andtritium in water. Isot Environ Health Stud 45:83–95

Thorweihe U (1982) Hydrogeolgie des DakhlaBeckens. Reihe A/Band 38. Verlag von Dietrich Reimer, Berlin

Thorweihe U, Heinl M (2002) Groundwater resources of the Nubian Aquifer System, NE-Africa. Modified synthesis submitted to: observatoire du Sahara et du Sahel. OSS, Paris, pp 23

Weiss RF (1970) The solubility of nitrogen, oxygen and argon in water and seawater. Deep Sea Res OceanogrAbstr 17:721–735

Weiss RF, Kyser TK (1978) Solubility of krypton in water and sea water. J ChemEng Data 23:69–72. https://doi.org/10.1021/je60076a014

Winckler G, Aeschbach-Hertig W, Kipfer R, Botz R, Rübel AP, Bayer R, Stoffer P (2001) Constraints on origin and evolution of Red Sea brines from helium and argon isotopes. Earth Planet SciLett 184:671–683